**JSWSC**

Available online at:
www.swsc-journal.org

**RESEARCH ARTICLE**

**OPEN 𝛛 ACCESS**

# Occurrence rate and duration of space weather impacts on high-frequency radio communication used by aviation

Robyn A. D. Fiori[1,*] ⓘ, Vickal V. Kumar[2], David H. Boteler[1] ⓘ, and Michael B. Terkildsen[2]

[1] Canadian Hazards Information Service, Natural Resources Canada, Ottawa, K1A 0E7 ON, Canada
[2] Space Weather Services, Australian Bureau of Meteorology, Sydney, 2010 New South Wales, Australia

**Abstract** – High frequency (HF) radio wave propagation is sensitive to space weather-induced ionospheric disturbances that result from enhanced photoionization and energetic particle precipitation. Recognizing the potential risk to HF radio communication systems used by the aviation industry, as well as potential impacts on GNSS navigation and the risk of elevated radiation levels, the International Civil Aviation Organization (ICAO) initiated the development of a space weather advisory service. For HF systems, this service specifically identifies shortwave fadeout, auroral absorption, polar cap absorption, and post-storm maximum useable frequency depression (PSD) as phenomena impacting HF radio communication and specifies moderate and severe event thresholds to describe event severity. This paper examines the occurrence rate and duration of events crossing the moderate and severe thresholds. Shortwave fadeout was evaluated based on thresholds in the solar X-ray flux. Analysis of 40-years of solar X-ray flux data showed that moderate and severe level solar X-ray flares were observed, on average, 123 and 5 times per 11-year solar cycle, respectively. The mean event duration was 68 min for moderate level events and 132 min for severe level events. Auroral absorption events crossed the moderate threshold for 40 events per solar cycle, with a mean event duration of 5.1 h. The severe threshold was crossed for 3 events per solar cycle with a mean event duration of 12 h. Polar cap absorption had the longest mean duration at ~8 h for moderate events and 1.6 days for severe events; on average, 24 moderate and 13 severe events were observed per solar cycle. Moderate and severe thresholds for shortwave fadeout, auroral absorption, and polar cap absorption were used to determine the expected impacts on HF radio communication. Results for polar cap absorption and shortwave fadeout were consistent with each other, but the expected impact for auroral absorption was shown to be 2–3 times higher. Analysis of 22 years of ionosonde data showed moderate, and severe PSD events occurred, on average, 200 and 56 times per 11-year solar cycle, respectively. The mean event duration was 5.5 h for moderate-level events and 8.5 h for severe-level events. During solar cycles 22 and 23, HF radio communication was expected to experience moderate or severe impacts due to the ionospheric disturbances caused by space weather, a maximum of 163 and 78 days per year, respectively, due to the combined effect of absorption and PSD. The distribution of events is highly non-uniform with respect to the solar cycle: 70% of moderate or severe events were observed during solar maximum compared to solar minimum.

**Keywords:** Space weather / radio wave propagation / ionosphere / aviation

## 1 Introduction

The term "space weather" describes processes, starting on the Sun that causes disturbances in the space environment, geomagnetic field, and Earth's ionosphere and thermosphere. Enhanced ionization in the ionosphere due to photoionization and energetic particle precipitation due to magnetospheric–ionospheric coupling, which can be intensified during periods of heightened solar activity, leads to ionospheric disturbances (e.g., Davies, 1990; Newell et al., 2001). These disturbances can affect high frequency (3–30 MHz; HF) radio wave communication (HF COM) used by the aviation industry (e.g., Coyne, 1979; Davies, 1990; Goodman, 1992; Newell et al., 2001, Hunsucker & Hargreaves 2003; National Research Council, 2008; Cannon et al., 2013; Boteler, 2018; Knipp et al., 2021).

Propagation of radio signals is strongly dependent on ionospheric electron density, which determines whether a transmitted signal will be absorbed in the D-region ionosphere, be

---

*Corresponding author: robyn.fiori@nrcan-rncan.gc.ca

reflected in the E or F-region ionosphere back toward the ground (HF COM), or be transmitted entirely through the ionosphere (SATCOM) (Davies, 1990). The range of frequencies suitable for HF COM is bounded by the lowest usable frequency (LUF) and the maximum useable frequency (MUF). Transmissions lower than the LUF are absorbed in the ionosphere, and transmissions higher than the MUF penetrate the ionosphere and are not reflected. The climatology of ionospheric electron densities, and therefore the routine LUFs and MUFs for a radio path, are regulated by diurnal, seasonal, and solar cycle factors as photoionization by solar radiation changes with time of day, season, and phase of the solar cycle. Deviations in the ionospheric electron density caused by ionospheric disturbances shift the range of usable frequencies by either raising the LUF and/or lowering the MUF. Strong space weather disturbances can shift the LUF and/or MUF such that HF radio communication is seriously degraded or entirely unusable.

The International Civil Aviation Organization (ICAO) recognizes space weather as a hazard to aviation with potential impacts on HF COM and GNSS services and impacts from radiation (ICAO, 2018, 2019). ICAO initiated the development of an operational space weather advisory service to alert aviation operators to hazardous space weather conditions. This 24/7 service began operation on 07 November 2019 and is produced, in rotation, by 4 global warning centers: the Australia–Canada–France–Japan consortium (ACFJ), the China–Russia Consortium (CRC), the Partnership of Excellence for Civil Aviation Space Weather User Services (PECASUS; Kauristie et al., 2021) (Finland, Belgium, United Kingdom, Poland, Germany, Netherlands, Italy, Austria, Cyprus, and South Africa), and the National Oceanic and Atmospheric Administration (NOAA) Space Weather Prediction Center (SWPC) (United States). Space weather advisories produced by these global centers are distributed via the ICAO Aeronautical Fixed Telecommunication Network (AFTN) to users in the same way as meteorological aviation advisories.

The ICAO space weather advisory service specifies thresholds where moderate and severe space weather impacts are expected for HF COM. This paper evaluates the occurrence rate and duration of threshold crossing events to support infrastructure operators and industry in protecting against and mitigating the effects of space weather on aviation. Section 2 describes the space weather phenomena likely to affect HF COM. Event thresholds for each space weather phenomenon are described in Section 3. Section 4 presents the frequency and duration of the space weather events that exceed the specified thresholds for each phenomenon.

## 2 Space weather phenomena affecting HF COM

Space weather phenomena impact HF COM by narrowing the window of useable frequencies: either through an increase of D-region absorption raising the LUF or reduction of E and F region electron density lowering the MUF. Correctly identifying the source of the HF COM impact determines whether a shift to higher or lower frequencies is necessary to continue using HF COM. In severe cases, the LUF or MUF shifts so

dramatically the frequency window is reduced to zero such that communication is not possible: a condition referred to as a "radio blackout".

The primary phenomena affecting HF COM are absorption and post-storm MUF depression (PSD). This section starts by describing the three primary types of absorption and then examines PSD.

### 2.1 Absorption

HF signals are subject to absorption in the D-region ionosphere due to the interaction of radio waves with ionospheric particles. Energy from the radio waves is transferred to charged particles in the ionosphere and can be lost through collisions with neutral particles before being reradiated. The D-region ionosphere has a high neutral particle density compared to the upper E and F-regions of the ionosphere. This higher neutral particle density results in an increased rate of particle collisions, causing radio waves to be dispersed or absorbed, as heat, thereby reducing signal strength. Enhancements in the D-region electron density, often caused by space weather, lead to increased absorption. There are three primary types of absorption affecting HF COM: shortwave fadeout, auroral absorption, and polar cap absorption.

#### 2.1.1 Shortwave fadeout (SWF)

Solar X-ray flares are a sudden brightening of the solar photosphere accompanied by an emission of electromagnetic radiation, most notably in the X-ray and EUV bands (e.g., Mitra, 1974; Davies, 1990). The enhanced radiation increases photoionization on the sunlit side of the Earth, enhancing the electron density (Belrose & Cetiner, 1962; Davies, 1990). A direct result is the increased absorption of shortwave radio signals, commonly referred to as shortwave fadeouts (e.g., Mitra, 1974). The amount of absorption is related to the solar zenith angle and is most pronounced in the dayside ionosphere at equatorial latitudes and falls off toward dawn and dusk (e.g., Davies, 1990). Shortwave fadeout is characterized by a sudden reduction in the signal strength followed by a more gradual recovery and closely follows the timescales of the solar flare radiation (Davies, 1990). Larger magnitude solar X-ray flares are associated with stronger SWF events.

Magnitudes of solar X-ray flares are classified using a letter-based system based on the peak intensity of the solar X-ray flux ($F_{\text{peak}}$) measured in the 0.1–0.8 nm band. A, B, C, M, and X-class flares represent a solar X-ray flux of $F_{\text{peak}} < 10^{-7}$ Wm$^{-2}$, $10^{-7} \leq F_{\text{peak}} < 10^{-6}$ Wm$^{-2}$, $10^{-6} \leq F_{\text{peak}} < 10^{-5}$ Wm$^{-2}$, $10^{-5} \leq F_{\text{peak}} < 10^{-4}$ Wm$^{-2}$, and $F_{\text{peak}} \geq 10^{-4}$ Wm$^{-2}$, respectively. The size of a flare is given by the flux value, using the classification letter as a multiplier. For example, an X4.5 flare has a peak flux of $4.5 \times 10^{-4}$ Wm$^{-2}$. Flare duration is related to flare intensity. The expected recovery time following a solar flare peak for M, X1, and X5 solar X-ray flares are 25, 60, and 120 min, respectively (https://www.swpc.noaa.gov/content/global-d-region-absorption-prediction-documentation) (last accessed, 16 December 2021).

There are numerous examples in the literature of SWF impacting HF systems and HF COM. Impacts to HF systems

are clearly demonstrated in flare-time signatures seen in measurements from the Super Dual Auroral Radar Network (SuperDARN) (e.g., Hosokawa et al., 2000; Watanabe & Nishitani, 2013; Berngardt et al., 2018; Chakraborty et al., 2018; Fiori et al., 2018). SWF impacts on the Reverse Beacon Network (RBN) and the Weak Signal Propagation Reporting Network (WSPRNet), operating at 6 bands spanning 1.8– 28 MHz, are demonstrated in Frissell et al. (2014). During the September 2017 space weather event, SWF impacted HF COM used for emergency communications affecting hurricane relief efforts associated with hurricanes Irma and Jose (Redmon et al., 2018; Frissell et al., 2019).

### 2.1.2 Auroral absorption (AA)

The D-region ionosphere is sensitive to the precipitation of high energy (>30 keV) magnetospheric electrons driven by the solar wind-magnetosphere–ionosphere interaction. This energetic electron precipitation can be intensified during space weather events leading to enhanced ionization in the ionosphere at auroral latitudes, causing a phenomenon known as auroral absorption (e.g., Hargreaves, 1969; Baker et al., 1981; Newell et al., 2001; Fiori et al., 2020). Auroral absorption peaks between 64° and 68° geomagnetic latitude in the pre-midnight sector due to electron precipitation and in the pre-noon sector due to the eastward drift of diffuse auroral electrons (Basler, 1963; Hartz et al., 1963; Driatsky, 1966; Hargreaves, 1969, 2010; Kavanagh et al., 2004; Tesema et al., 2020). Events last approximately 1–3 h (Hargreaves, 2010).

Auroral absorption is typically observed during periods of enhanced geomagnetic activity (e.g., Hargreaves, 1969) and can be characterized using various geomagnetic activity indices such as the PC index (Frank-Kamenetsky & Troshichev, 2012), the mid-latitude positive bay index (Sergeev et al., 2020), the hourly range of the magnetic field (Fiori et al., 2020), and more commonly the Kp or Ap index (e.g., Holt et al., 1961; Hargreaves, 1966; Hargreaves & Cowley, 1967; Foppiano & Bradley, 1983, 1984; Kavanagh et al., 2004).

Figure 1 illustrates the poleward and equatorward edges of the auroral zone for strong levels of geomagnetic activity (Kp = 8 and Kp = 9) in a magnetic latitude (MLAT)/magnetic local time (MLT) (sun-oriented) coordinate system. Note the almost perfect overlap of the contours indicating very little change in the region expected to be impacted by Kp = 8 and Kp = 9 events. Based on this image, the region impacted by auroral absorption is expected to be skewed toward the nightside. During strong periods of geomagnetic activity, the auroral zone is confined to a band of latitudes, primarily poleward of 60° MLAT and equatorward of 85° MLAT on the nightside. On the dayside, the auroral zone is shifted to higher latitudes, mostly between 75° and 85° MLAT.

It should be noted that contours for the auroral oval presented in Figure 1 are based on the Starkov (1994) auroral boundary model, as summarized in Sigernes et al. (2011). This model is based on data from all-sky images and represents the boundary of the visual auroral. Although there should be a rough overlap between the boundary of the visual aurora, and the region expected to be impacted by auroral absorption, there may not always be a one-to-one correspondence as the visual aurora are not always caused by the same electrons that cause auroral absorption.
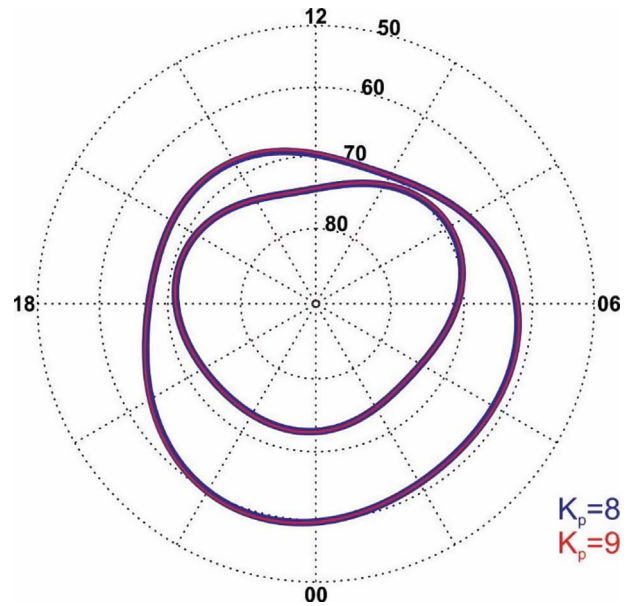


**Fig. 1.** Poleward and equatorward edge of the auroral oval modeled using the Starkov (1994) auroral boundary model as summarized in Sigernes et al. (2011). Boundaries are plotted for Kp = 8 (blue) and Kp = 9 (red) in magnetic latitude/magnetic local time coordinates. Because of the almost perfect overlap of the contours, the Kp = 8 boundary is plotted with a thicker line. Dashed lines indicate a magnetic latitude in 10° increments and magnetic local time in 2-h increments. Kp = 8 and Kp = 9 were chosen to represent moderate and severe activity, as described by the ICAO thresholds for auroral absorption, see Section 3.

### 2.1.3 Polar cap absorption (PCA)

Solar energetic protons expelled at the same time as a solar flare or coronal mass ejection (CME) can be accelerated to near relativistic speeds, reaching the Earth within a few hours. The solar energetic protons penetrate down to D-region altitudes in the high-latitude region reaching as equatorward as 60–65° MLAT causing polar cap absorption (PCA) (e.g., Hargreaves et al., 1993; Kavanagh et al., 2004; Hargreaves, 2005; Kouznetsov et al., 2014). This form of absorption is more strongly felt in the high-latitude sunlit ionosphere leading to a solar zenith angle dependence on the level of absorption, with strongest impacts near local noon falling off toward the terminator. Of all the forms of absorption, PCA is the most problematic for HF radio communication as it can be a relatively long-lived phenomenon lasting on the order of days. Threats due to PCA have diverted transpolar flights between North America and Asia (NOAA, 2004; National Research Council, 2008; Cameron, 2012). PCA is of particular concern for trans-polar flights as alternative means of communication, such as geosynchronous satellites or VHF radio links, are not available due to geometry or a lack of infrastructure.

### 2.2 Post storm maximum usable frequency depression (PSD)

The upper limit of the HF frequency window, described by the MUF, is dependent on the F region electron density profile.

**Table 1.** Parameters and activity levels describing MOD and SEV level activity for shortwave fadeout (SWF), auroral absorption (AA), polar cap absorption (PCA), and post-storm maximum usable frequency depression (PSD) based on ICAO regulations (ICAO, 2019).

| Sub-effect | Parameter | MOD | SEV |
|---|---|---|---|
| SWF | Solar X-ray flux (0.1–0.8 nm wavelength) ($Wm^{-2}$) | $1 \times 10^{-4}$ (X1) | $1 \times 10^{-3}$ (X10) |
| AA | $Kp$ index | 8 | 9 |
| PCA | Absorption at 30 MHz (dB) | 2 | 5 |
| PSD | MUF* | 30% | 50% |

* Compared to a 30-day running median of the critical frequency of the foF2.

After the onset of a geomagnetic storm, F-region electron densities can reduce below quiet-time values (negative storm effect). Negative storm effects can last for several tens of hours (see reviews by Buonsanto, 1999; Prölss, 1995, 2008; Mendillo, 2006; Danilov, 2013, and references therein) and can cause difficulties for HF radio links operating at higher frequencies. Geomagnetic storms can also cause F region electron density enhancements (positive storm effect). Positive storm effects are not detrimental to HF systems.

Negative storm effects are associated with the depletion of the atomic oxygen to molecular nitrogen ratio [O]/[N$_2$] in the lower auroral thermosphere caused by storm-induced Joule and precipitating particle heating (e.g., Lu et al., 2001; Prölss & Werner, 2002). As the neutral gas becomes more molecular, the recombination rate is increased, and the ambient ionospheric electron density decreases. The auroral heating also drives enhanced equatorward winds that transport the depleted O/N$_2$ gas equatorward. The equatorial limit of the negative storm effect is regulated by the superposition of two large-scale thermospheric circulation systems: the storm-induced winds (dependent on storm intensity) and the background solar-induced winds (varying with season and local time) (e.g., Fuller-Rowell et al., 1996; Danilov, 2013).

Even though the negative storm mechanism is generally well understood, it remains difficult to predict when, where, and how strong the negative ionospheric storm effect will be. In general, negative storm effects first occur on the nightside auroral and sub-auroral zones; the magnitude of depressions and the extent of their equatorward expansion increases with increasing storm intensity. These depressions occur in all seasons but are least likely in winter (e.g., Fuller-Rowell et al., 1996; Tulasi Ram et al., 2010; Kumar & Parkinson, 2017).

The maximum electron density of the ionosphere and the height at which these maximum electron densities occur can be extracted from ground-based ionosonde observations and also derived from satellite observations using radio occultation techniques (e.g., Cherniak et al., 2021). Ionosondes measure the critical frequency of the F2 layer (foF2), which is equivalent to the MUF at vertical incidence. Ionosonde soundings can also be used to determine the MUF for a 3000 km radio link, commonly known as MUF(3000)F2. Assimilation of the observations from the sparsely distributed global ionosonde network with the international reference ionospheric model (Bilitza et al., 2017) are widely used to generate global MUF maps.

# 3 ICAO guidelines for issuing HF COM space weather aviation advisories

Requirements for issuing space weather advisories for aviation are outlined in ICAO (2018). HF COM space weather advisories are issued to provide a general description of the time period and region where communications are expected to be impacted by space weather. For HF COM, advisories are issued for space weather impacts associated with SWF, AA, PCA, and PSD. The severity level (moderate – MOD; severe – SEV) of the activity is based on ICAO-defined thresholds for parameters characterizing the different HF COM phenomena (see Table 1).

SWF thresholds are based on the amplitude of the 0.1–0.8 nm wavelength solar X-ray flux, measured by the NOAA/NASA Geostationary Orbital Environmental Satellites (GOES). MOD and SEV level thresholds are set at > X1 and > X10 solar X-ray flares, respectively. Thresholds for MOD and SEV auroral absorption are specified using the Kp index, which identifies periods of strong geomagnetic activity likely to be associated with strong auroral absorption. MOD and SEV thresholds are set at Kp = 8 and Kp = 9, respectively. PCA thresholds are based on the absorption expected for a 30 MHz signal. The MOD-level absorption threshold is 2 dB, and the SEV-level threshold is 5 dB. The thresholds for MOD and SEV PSD are described by a 30% or 50% drop in MUF compared to the 30-day running median value, provided a Kp index of Kp $\geq$ 6 was observed during the previous 96 h. Under MOD conditions, HF COM is expected to be degraded, whereas under SEV conditions, HF COM is expected to be entirely unreliable.

# 4 Occurrence rate and duration of events

In this section, the occurrence rate and duration of typical SWF, AA, PCA, and PSD events are evaluated using data collected between 1980 and 2020. The event occurrence rate tends to demonstrate trends that closely follow the solar activity cycle indicated in Figure 2a by the 13-month smoothed sunspot number. Data in Figure 2 spans three complete solar cycles: solar cycle 22 (1986–1995), 23 (1996–2007), and 24 (2008–2018). Years in each cycle were roughly split in two, representing years of solar maximum and solar minimum based on the inclination and declination of the sunspot number. In Figure 2a, years of solar maximum are indicated by grey shading.
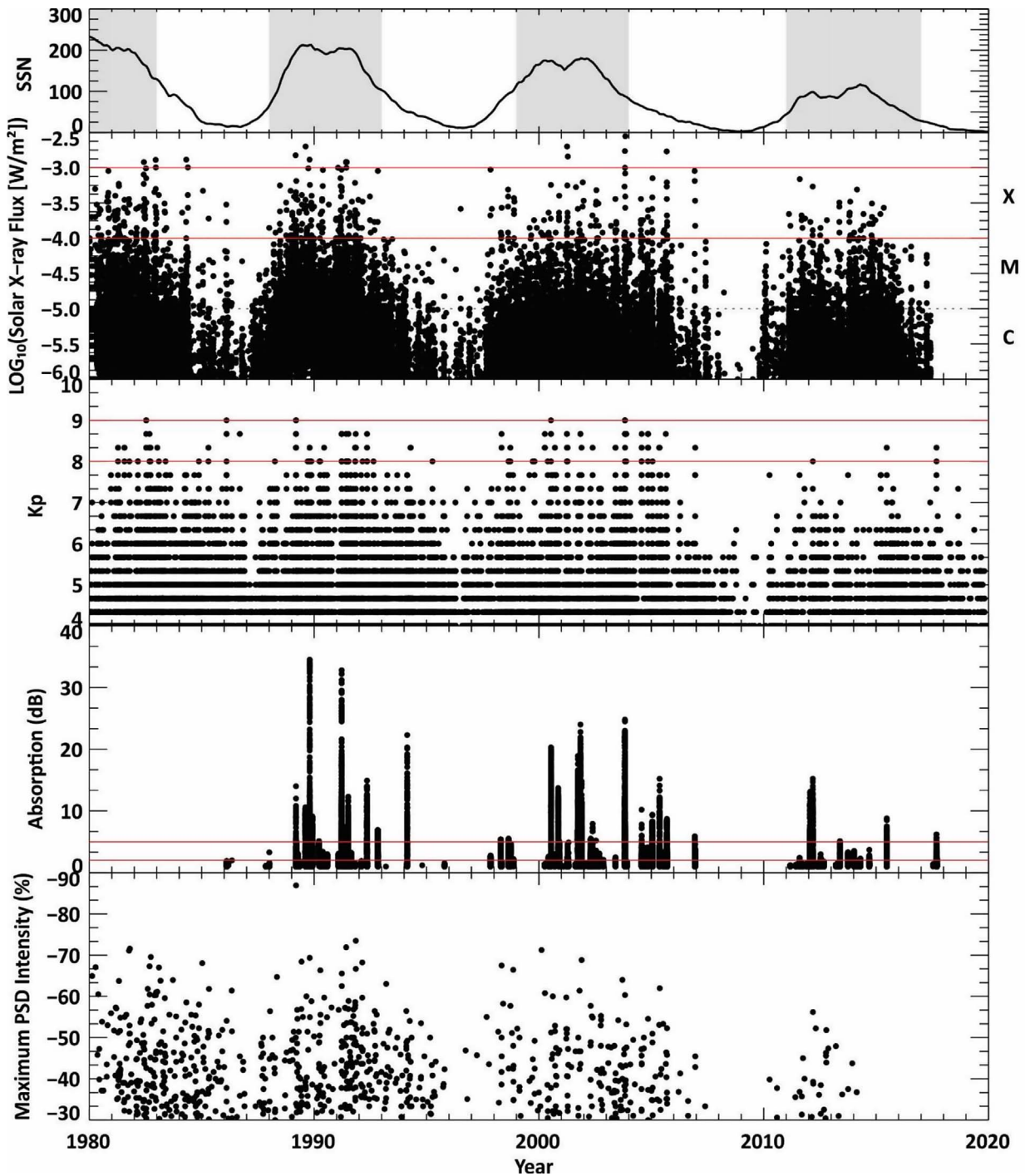
**Fig. 2.** (a) The 13-month smoothed mean total sunspot number. Grey shading indicates solar maximum years. Occurrence of (b) solar X-ray flux for 01 January 1980 until 28 June 2017, (c) Kp for 1980–2020, and (d) D-RAP modelled absorption >1 dB for all PCA event observed in 1986–2020. Red horizontal lines indicate MOD and SEV event thresholds for (b) SWF (X1 and X10 solar X-ray flare), (c) AA (Kp = 8, 9), and (d) PCA (2 dB and 5 dB absorption at 30 MHz). (e) Maximum intensity of PSD events, represented by hourly relative foF2.

## 4.1 Shortwave fadeout

The first SWF advisory issued through the auspices of ICAO was in response to an X1.6 solar X-ray flare that erupted off the western edge of the solar disc on 03 July 2021. This is a significant event as it was the first observed since September

2017 and marks the first X-class solar X-ray flare of Solar Cycle 25. Figure 3 plots the absorption observed for a 30 MHz signal by the Alert (ALE), Resolute Bay (RES), Clyde River (CLY), Cambridge Bay (CBB), Iqaluit (IQA), Yellowknife (YKC), Meanook (MEA), and Ottawa (OTT) Canadian riometers. This riometer array was advantageously positioned on the dayside
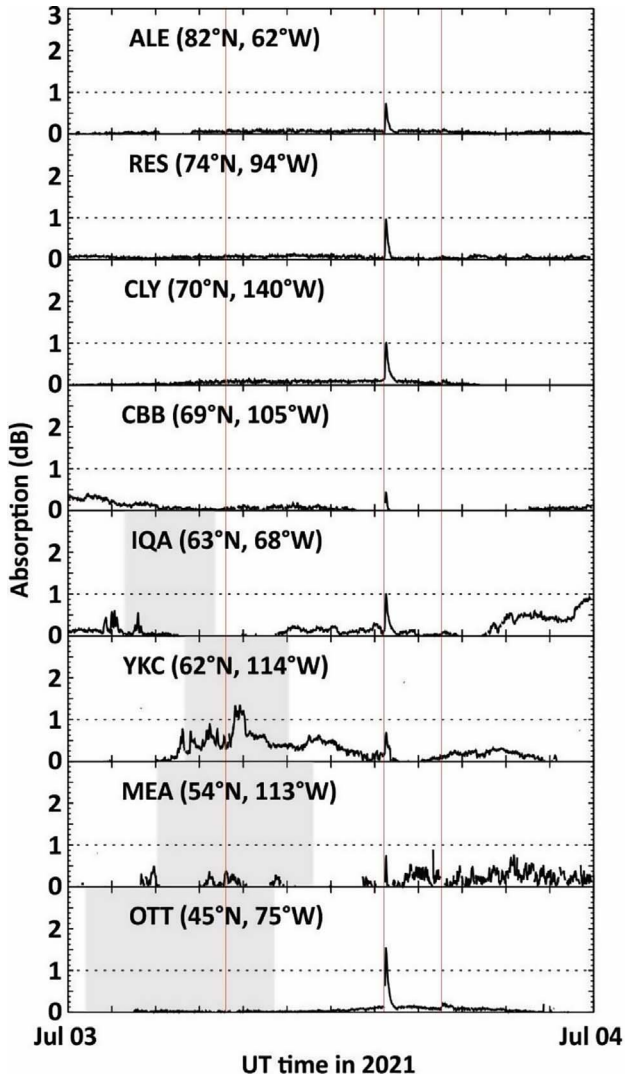
**Fig. 3.** Absorption at 30 MHz observed by Canadian riometer stations at the geographic coordinates noted. Grey shading indicates the time between sunset and sunrise when the station was located on the nightside. Red vertical lines indicate the onset, from left to right, of an M2.7, X1.6, and M1.0 solar X-ray flare.

and observed a clear response to the event X1.6 solar X-ray flare shortly after 14 UT. Although SWF is strongest at low latitudes, an absorption response, peaking at 0.74 dB, was observed even at the northernmost station (ALE) at 82° N geographic latitude. Absorption peaked for all stations 1–2 min after the X1.5 peak at 14:29 UT. The maximum absorption of 1.6 dB was observed by the lowest latitude riometer (OTT) at 45° N geographic latitude. Absorption at 30 MHz scales by frequency (Davies, 1990):

$$A_f = \left(\frac{30\,\text{MHz}}{f}\right)^2 A_{f_{30\,\text{MHz}}}. \tag{1}$$

At Ottawa, absorption of 1.6 dB would then scale to 14.4 dB at 10 MHz and 57.6 dB at 5 MHz, which are within the range of HF COM used for aviation. Minor absorption enhancements are

observed at ~17 UT in response to the lower magnitude M1.0 solar X-ray flare. No response is observed for the ~7 UT flare observed while lower latitude stations were on the nightside. Note the absorption observed from 04–14 UT at YKC is attributed to auroral absorption, not shortwave fadeout.

It should be noted that there is some debate in the literature over the exponent of 2 present used to scale absorption by frequency in equation (1). Stonehocker (1970) and Schwentek (1961) report a factor of 2 as a theoretical expectation for purely nondeviative absorption. However, in a more realistic scenario where nondeviative absorption is likely to be mixed with deviative absorption, the factor varies. Sauer & Wilkinson (2008) and Schumer (2009) recommend exponents of 1.5 and 1.24, respectively. Zaalov & Moskaleva (2016) propose a more complex exponent that is a function of the *f*.

The occurrence rate of solar X-ray flares for 1980–2020 is illustrated in Figure 2b, and summarized in Table 2. Data are taken from the GOES X-ray sensor reports (XRS) (https://www.ngdc.noaa.gov/stp/space-weather/solar-data/solar-features/solar-flares/x-rays/goes/xrs/, which contain information on flare magnitudes, the timing of the start, peak, and end of the flare, and solar coordinates of the eruption. See, for example, Swalwell et al. (2018) for information on how these parameters are defined. All data entries were used, provided the event times were recorded. Data were available until 28 June 2017. The distribution of the 51,608 ≥ C flares represented in Figure 2b is consistent with the rise and fall of solar activity characterizing the solar cycle. Ignoring the A and B flares, which are not of interest for this study, the C-class flares are the vast majority (87.8%). M-class and X-class flares are primarily limited to years surrounding solar maximum, with some years not observing any M or X-class solar X-ray flares. There are 5840 (11.3%) M-class and 438 (0.8%) X-class solar X-ray flares. If the X-class flares are further divided, there are 420 ≥ X1 and < X10 flares (MOD-level SWF) and 18 ≥ X10 flares (SEV-level SWF) observed. Based on the 37.5-year period of observation, this corresponds to an average of 123 MOD and 5 SEV events, non-uniformly distributed across the 11-year solar cycle with a peak occurrence rate near the solar maximum. The largest flare reported in this data set is an X28 flare observed on 04 November 2003 with onset, peak, and end time of 19:29 UT, 19:50 UT, and 20:06 UT, respectively. Brodrick et al. (2005) report that the sensor saturated for this event and, through a careful analysis of riometer data, showed the flare was likely X40 in magnitude.

Event duration was determined from the start and end times recorded in the GOES XRS files. Table 2 records the minimum, maximum, and mean duration observed for the events. C-class events show the most variability ranging from <1-min to 728 min duration. Based on the mean duration of 22 min (median of 15 min), they are the shortest-lived event. M-class flares range from <1-min to 573 min, with a mean duration of 43 min and a median duration of 29 min. MOD-level solar X-ray flares range from 3 to 528 min with a mean duration of 68 min and a median duration of 48 min. SEV-level solar X-ray flares have durations that are strictly >30 min, with a mean duration of 132 min and a median duration of 96 min. These values are in agreement with total flare recovery times reported by NOAA SWPC (https://www.swpc.noaa.gov/content/global-d-region-absorption-prediction-documentation),

**Table 2.** Occurrence and duration of SWF, AA, PCA, and PSD events overall and for a subset of MOD and SEV events. See the text for additional details.

| SWF | Flare class | Occurrence | Occurrence $\geq$ C | Event duration (minutes) | | | |
|---|---|---|---|---|---|---|---|
| | | | | Min | Max | Mean | Median |
| | C | 45,330 | 87.8% | 0 | 728 | 22 | 15 |
| | M | 5840 | 11.3% | 0 | 573 | 43 | 29 |
| | X1 (MOD) | 420 | 0.8% | 3 | 528 | 68 | 48 |
| | X10 (SEV) | 18 | 0.03% | 31 | 464 | 132 | 96 |

| AA | *Kp* | Occurrence | Occurrence $\geq$ 4 | Event duration (hours) | | | |
|---|---|---|---|---|---|---|---|
| | | | | Min | Max | Mean | Median |
| | 4 | 8998 | 64.2% | – | – | – | – |
| | 5 | 3342 | 23.8% | – | – | – | – |
| | 6 | 1133 | 8.1% | – | – | – | – |
| | 7 | 403 | 2.9% | – | – | – | – |
| | 8 (MOD) | 132 | 0.9% | 3 | 15 | 5.1 | 3 |
| | 9 (SEV) | 9 | 0.1% | 6 | 21 | 12.0 | 12 |

| PCA | Absorption (dB) | Occurrence | Occurrence $\geq$ 1 dB | Event duration (hours) | | | |
|---|---|---|---|---|---|---|---|
| | | | | Min | Max | Mean | Median |
| | $1 \leq A < 2$ (MOD) | 27,418 | 53.2% | – | – | – | – |
| | 2 (MOD) $\leq A < 5$ (SEV) | 17,490 | 33.9% | 0.25 | 39.42 | 7.85 | 4.92 |
| | $A \geq 5$ (SEV) | 6657 | 12.9% | 3.08 | 176.75 | 39.18 | 35.83 |

| PSDs | $\Delta$foF2 | Occurrence | | Event duration (hours) | | | |
|---|---|---|---|---|---|---|---|
| | | | | Min | Max | Mean | Median |
| | $-30\% \geq \Delta$foF2 $> -50\%$ (MOD) | 727* | | 2 | 96 | 5.47 | 3 |
| | $-50\% \geq \Delta$foF2 (SEV) | 203* | | 2 | 54 | 8.54 | 8 |

which reports a duration of 25, 40, 60, and 120 min for an M1.0, M5.0, X1.0, and X5.0 solar X-ray flare, respectively.

In addition to examining the total duration of solar X-ray flares, the amount of time between X-class events and the amount of time elapsed between event peaks was examined. Over the 40-year period, there were only two events where >X1 solar X-ray flares occurred in close succession. Both events occurred in 1982 (X5.9 and X2.4 flares 04 June; X9.8 and X1.1 flares on 09 July). The start of the second flare followed the end of the first flare by 2 and 1 min, respectively. The time between the peaks of the flare pairs was 105 and 52 min, respectively. Examination of the time of the peak of all >X1 solar X-ray flares showed there is a minimum separation of 1 min between successive flares, with a mean separation of 29 days and a median separation of 3 days. The maximum interval between successive X-class flares was 1523 days, or ~4.2 years (during solar minimum).

## 4.2 Auroral absorption

Archived 3-h Kp data for 1980 to 2020 were examined using data files downloaded from the GFZ Potsdam (Matzka et al., 2021a, 2021b). Data were limited to periods where Kp $\geq$ 4. Figure 2c and Table 2 indicate the occurrence frequency of Kp $\geq$ 4 over this period. As with the SWF data illustrated in Figure 2b, the distribution of Kp follows solar cycle trends, with Kp $\geq$ 8 events observed more frequently during solar maximum. For the Kp $\geq$ 4 subset of all Kp data from 1980 to 2020, 99% of 3-h increments observed $4 \leq$ Kp $\leq 7$. There are 132 MOD (Kp = 8) and 9 SEV (Kp = 9) level 3-h increments, representing 0.9% and 0.1% of the data set.

Intervals of Kp $\geq$ 8 were grouped into events. An event was defined as a group of one or more consecutive 3-h intervals containing no more than a single 3-h gap. Most events had consecutive 3-h intervals with Kp $\geq$ 8, and only 5 events contained a 3-h gap. Figure 4 illustrates the onset, duration, and magnitude for all Kp $\geq$ 8 events (one entry per event). Three-hour blocks where Kp was enhanced at MOD and SEV levels are indicated by orange and red shading, respectively. For the purpose of this analysis, an event that contains at least one interval of SEV-level activity is classified as "SEV", even if the other 3-h intervals in the event do not contain SEV activity levels. All other Kp $\geq$ 8 events are classified as "MOD". Over the entire 40-year interval, 78 events were observed, representing 438 h of MOD or SEV level activity. Of these, 72 events and 366 h were MOD, and 6 events and 72 h were SEV. Event duration ranged from 3 to 15 h for MOD-level events, with a mean duration of 5.1 h and a median duration of 3 h. Event duration ranged from 6 to 21 h for SEV-level events, with a mean and median duration of 12 h. The longest-lasting event was observed on 13–14 March 1989, where auroral absorption was at MOD levels (8 $\leq$ Kp < 9) from 06–21 UT and above the SEV threshold (Kp $\geq$ 9) from 21–03 UT. The largest number of events per year was observed in 1991; 11 MOD-level events and 78 h of enhanced activity represented 18% of the data set.

In addition to examining event duration, the interval between events was also evaluated. The mean separation between events was 177 days. The minimum event separation of 6 h was observed for 6 different events. A separation of <1 day was observed for 12 events. The maximum event separation of 1911.125 days (~5 years) was observed between 3-h
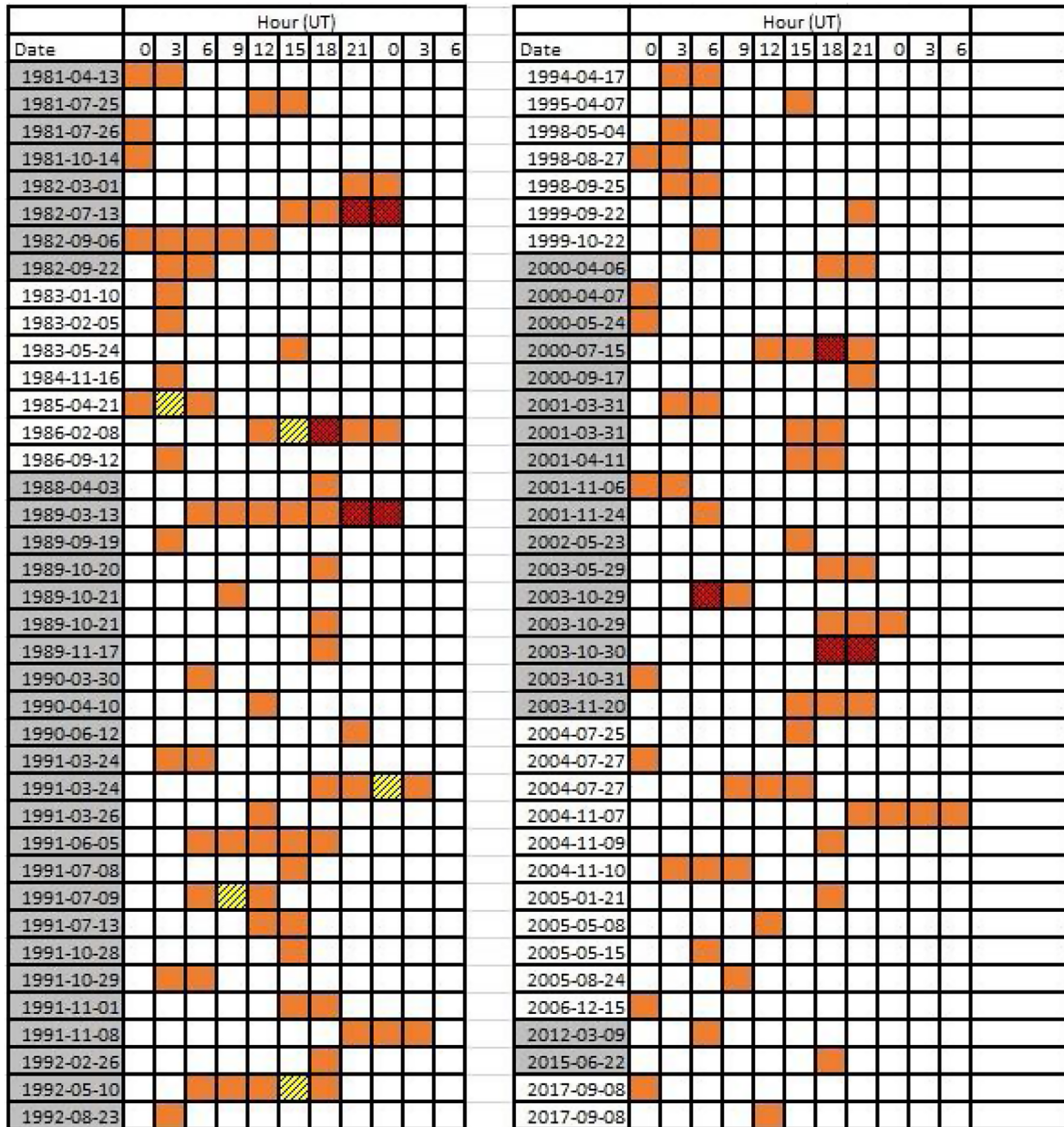
**Fig. 4.** Date and time (in UT-hour) of MOD and SEV level AA based on Kp-index. Each block represents a 3-h period. Orange (solid) and red (crosshatched) shading indicate MOD and SEV level activity. Yellow (diagonal striped) shading indicates a 3-h gap in MOD or SEV activity observed during an event. Each line represents a different event. Grey shading indicates events observed during solar maximum years, similar to Figure 2a.

events on 15 December 2006 and 09 March 2012, during the solar minimum between cycles 23 and 24.

## 4.3 Polar cap absorption

To evaluate PCA event frequency, it is necessary to know the PCA absorption maximum at regular intervals for more than one 11-year solar cycle. As such a data set does not exist within the Natural Resources Canada (NRCan) riometer network evaluated, this paper relies on the D-Region Absorption Prediction (D-RAP) model (Sauer & Wilkinson, 2008), D-RAP is primarily based on the integral proton flux derived from GOES

satellite measurements, but also incorporates geomagnetic activity through the use of the Kp and SYM-H indices, geomagnetic latitude, and solar zenith angle. For this study, a list of PCA events was determined by evaluating the maximum D-RAP absorption at 5-min increments during periods surrounding solar proton events (SPE) recording in the SPE event list maintained by NOAA SWPC (ftp://ftp.swpc.noaa.gov/pub/indices/SPE.txt). Each entry for 1986–2020, plus the subsequent 9 days for each entry, wase evaluated at 5-min increments along a uniformly distributed grid of points having a grid spacing of 2° at geographic latitudes >50°. Figure 2d and Table 2 indicate the occurrence frequency of PCA events with absorption, A, below the

MOD threshold (1 dB $\leq A <$ 2 dB), exceeding the MOD threshold but not exceeding the SEV threshold (MOD; 2 dB $\leq A <$ 5 dB), and exceeding the SEV threshold (SEV; $A \geq$ 5 dB). As with other forms of absorption, the occurrence frequency of MOD and SEV level absorption is concentrated during periods of solar maximum, with long intervals between events during solar minimum. A total of 51,565 5-min intervals with $A \geq$ 1 dB were identified, representing only 0.16% of 5-min intervals in the entire 34-year period analyzed. Of these, 33.9% and 12.9% of 5-min intervals were MOD and SEV, respectively. The remaining 53.2% of the 5-min intervals with $A \geq$ 1 dB were below the MOD threshold.

Events were determined by grouping 3 or more consecutive 5-min intervals of $\geq$ 2 dB absorption, allowing a 3-h gap between consecutive points. For the purpose of this analysis, events were described as being either MOD or SEV based on the value of the maximum absorption. Over the 34-year period, 115 events were identified: 75 MOD and 40 SEV. This corresponds to 24 MOD and 13 SEV events, on average, per solar cycle, unevenly distributed, with more events occurring during solar maximum than the solar minimum. See Table A.1 for a list of events where absorption was modeled to exceed 2 dB.

Event duration for MOD-level events ranged from 0.25 to 39.42 h (1.6 days), with a mean duration of 7.85 h and a median duration of 4.92 h. SEV-level events were typically longer, with a range of 3.08–176.75 h (7.4 days), a mean duration of 39.18 h (1.6 days), and a median duration of 35.83 h (1.5 days), which is roughly equivalent to the maximum duration of the MOD level events observed. The maximum duration was observed for an event that began on 19 October 1989 at 15:35 UT and ended on 27 October 1989 at 00:20 UT and corresponds to the event having the highest observed absorption (34.5 dB) and >10 MeV solar proton flux ($4.22 \times 10^4$ pfu). The interval between consecutive events ranged from 3.25 h to 1695 days (4.6 years), with a median separation of 90 days. The largest gap observed was between 14 December 2006 and 05 August 2011.

### 4.4 Post-storm maximum usable frequency depression (PSD)

Evaluating the occurrence frequency of PSD events requires long-term global maps of MUFs. Specifically, these maps should be generated by assimilating real-time ionosonde observations. Such archives are difficult to find. As a compromise, this analysis is solely based on long-term observations from a global network of 72 selected ionosondes. These selected ionosondes all had data from more than 20 years.

The following describes the approach for identifying PSD events in ionosonde data: firstly, a monthly median diurnal curve at each ionosonde site is estimated from the data. This median curve describes, for each time point, the median foF2 at the given site and time over the previous 30 days. The foF2 values from the ionosonde are then expressed as a % deviation from this median curve.

The next step focuses only on data within 96 h following the onset of a Kp $\geq$ 6 storm event and identifies periods where the % deviations exceed the ICAO MOD and SEV thresholds. An additional criterion is applied as follows: If at least 2 successive hourly foF2 depression values were $\leq -30\%$ and at least one depression value was $\leq -50\%$, the event was classified as

SEV. If at least 2 successive hourly foF2 depression values were $\leq 30\%$ and neither was $\leq -50\%$, the event was classified as MOD. Once the MOD and SEV events were identified in individual ionosonde data, the events were combined into a "global" PSD event by identifying groups of ionosondes having overlapping depression events. The severity of the PSD event is assumed to be the highest depression level observed by the ionosonde group. The duration of the PSD event is assumed to be the time from when the relative foF2s first dropped below $\leq -30\%$ by any ionosonde within the group to the time when the relative foF2s were last below $\leq -30\%$ by any ionosonde within the same group.

The observation span of the available data from 72 ionosondes used in this analysis varied from 22 to 68 years. Figure 2e shows the occurrence frequency of MOD and SEV events from 1980 to 2020. Similar to absorption phenomena, event occurrence and magnitude shows a close relationship with the solar cycle, with more and larger events occurring during solar maximum.

Analysis of PSD events next focuses on data for solar cycles 22 and 23, extending from 1986 to 2008, as this period had the most continuous availability of ionosonde data. Over the 22-year period, 512 PSD events were observed: 400 MOD and 112 SEV. 29% of PSD events were solo events, that is, it was observed by only one ionosonde. A multitude of factors may have led to these solo events, such as large spatial distance between the ionosondes, occasional lack of concurrent observations from neighboring ionosondes, and several intrinsic factors. These factors include, for example, season, station location, local time of the station at storm onset, and storm time (prestorm, main phase, and recovery phase) which are known to affect ionospheric responses to storms (e.g., Buonsanto, 1999).

The variability in occurrence rate and duration of MOD and SEV PSD events over solar cycles 22 and 23 is shown in Figure 5. As expected, the PSD events were more common during the solar maximum since this time experienced more Kp $\geq$ 6 geomagnetic storms (Fig. 2). The occurrence rate of MOD and SEV PSD events was maximized at 12 events and 6 events per month, respectively. The most MOD PSD events in a month occurred in May 1991, and the most SEV PSD events were in September 1991. Most months during solar minima recorded 0 PSD events. The total duration of MOD and SEV conditions was 2186 h and 957 h, representing 1.1% and 0.5% of hours. The mean event duration of MOD and SEV PSD events was found to be 5.5 and 8.5 h, respectively. The total number of hours per month for MOD and SEV events ranged from 2 to 96 h and 2 to 54 h, respectively. Taking the worst case scenario, these results indicate that during a solar maximum month, such as May 1991, the upper limit of the HF communication band can be significantly impacted for 150 h (6 days) in the month.

## 5 Discussion

The number of absorption and PSD events expected per 11-year solar cycle is summarised in Table 3. Absorption is sub-divided into SWF, AA, and PCA. For each absorption sub-type, more MOD than SEV events are observed with ratios of 24.6, 10.0, and 1.8 for SWF, AA, and PCA, respectively. SWF events are characterized by the maximum solar X-ray flux
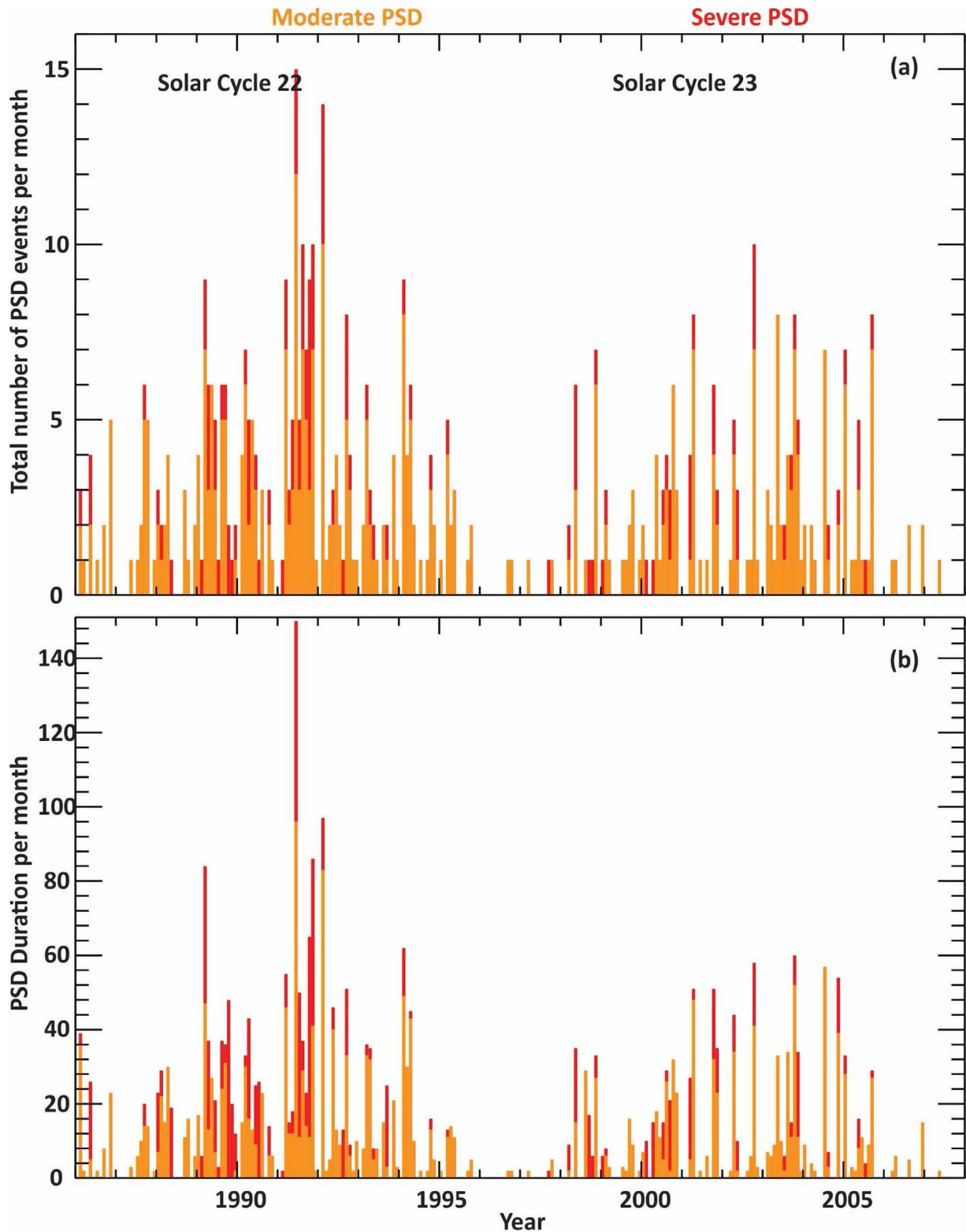
**Fig. 5.** Bar graph of (a) monthly total PSD events and (b) total number of PSD hours per month for solar cycle 22 and cycle 23. Amounts that are for moderate depression are shown in orange, and the remaining red shades represent severe depression.

observed during an event; an event can either be MOD or SEV, but not both. MOD and SEV AA, and PCA events were defined in this paper based on the maximum threshold crossed; for a SEV event, MOD and SEV activity are alternatively observed throughout the duration of an event. SWF events occur most frequently, with almost 3 times more events than either

**Table 3.** Events per 11-year solar cycle, average event duration, total duration per 11-year solar cycle, and equivalent absorption at 30 MHz for absorption (SWF, AA, and PCA) and PCA events.

| | Absorption | | | | | | PSD | | Total | |
| | SWF | | AA | | PCA | | | | | |
| | MOD | SEV | MOD | SEV | MOD | SEV | MOD | SEV | MOD | SEV |
|---|---|---|---|---|---|---|---|---|---|---|
| Events per 11-year solar cycle | 123 | 5 | 20 | 2 | 24 | 13 | 200 | 56 | – | – |
| Average event duration (hours) | 1.1 | 2.2 | 5.1 | 12 | 7.85 | 39.18 | 5.47 | 8.54 | – | – |
| Total duration per 11-year solar cycle (hours) | 135.3 | 11.0 | 102.0 | 24.0 | 188.4 | 509.34 | 1093 | 478.5 | 1518.7 | 1022.84 |
| Equivalent Absorption at 30 MHz (dB) | <3.6 | >3.6 | 4.3 | 13.8 | 2 | 5 | – | – | – | – |

AA or PCA. Although they have a higher occurrence rate, SWF events have the shortest duration, with MOD and SEV events lasting, on average, 1.1 and 2.2 h, respectively. AA events are roughly 5 times longer at 5.1 and 12 h. PCA events are the most long-lived, lasting, on average, 7.85 h for MOD events and >1.5 days for SEV events. The high occurrence rate of SEV PCA events per solar cycle compared to SWF and AA events, and a low MOD-to-SEV ratio indicates a high likelihood of solar protons being of high enough energy to cause a SEV-level event.

Like the absorption events, MOD PSD events occur more frequently than SEV events, with a ratio of ~4. The occurrence rate of PSD events is greater than the total occurrence rate of all types of absorption events. The average duration of MOD PSDs is comparable to that of a MOD AA or PCA event, while the average duration of SEV PSDs is greater than that of SWF but less than that of AA and PCA.

Table 3 also records the total duration of disturbed periods per 11-year solar cycle. Adding contributions from all space weather sources, 1621 h and 1035 h occur under a MOD-level and SEV-level advisory, respectively. Over the 11-year solar cycles, HF COM is at risk roughly 3% of the time due to space weather-produced absorption or PSD. Recognizing that there is likely to be some overlap in events, this number, of course, represents an absolute maximum. Also, note that the distribution of disturbances is not uniform, with MOD and SEV events heavily concentrated during solar maximum followed by periods of months, or even years when no advisories would be issued. If the event count for each phenomenon is split into periods of solar maximum and solar minimum, according to the shading in Figure 2a, then 84%, 68%, 74%, and 62% of SWF, auroral absorption, PCA, and PSD events occur during solar maximum periods.

MOD and SEV events are also non-uniformly distributed between solar cycles. Absorption events during the solar cycle 22 (1986–1995), 23 (1996–2007), and 24 (2008–2018) were counted and normalized based on the number of years in the solar cycle to determine the solar cycle distribution. SWF observed the highest proportion of events in solar cycle 22 at 51%. Auroral absorption was observed 47% of events during both solar cycles 22 and 23. PCA events were most commonly observed during solar cycle 23 at 48%. All 3 absorption phenomena observed a minimum occurrence frequency during solar cycle 24, ranging from 6% for auroral absorption events to 18% for PCA events. PSD events for solar cycles 22 and 23 showed a similar weighting of data, with 66% of events occurring during the more active solar cycle 22.

Another way of evaluating the data is the number of days during which at least one phenomenon caused an HF COM threshold to be crossed at least once during the day. Considering all event types during solar cycles 22 and 23, at least one event occurred between 15 (solar minimum) and 163 (solar maximum) days (mean = 57.5 days; median = 30.5 days) per year in solar cycle 22 and between 1 (solar minimum) and 78 (solar maximum) days (mean = 37.3 days; median = 41 days) per year in solar cycle 23. Roughly 3–4 times more events were observed during years of solar maximum compared to years of solar minimum for both solar cycles 22 and 23.

Absorption is a highly diverse phenomenon with different driving mechanisms. Although different parameters describe the potential for MOD and SEV impacts for each phenomenon, the actual impact itself is described by the absorption experienced by a signal at a given frequency. To normalize impacts, the equivalent absorption at 30 MHz is now determined.

The magnitude of absorption associated with MOD (X1 solar X-ray flare) and SEV (X10 solar X-ray flare) ICAO thresholds for SWF can be calculated based on the D-region absorption prediction (D-RAP) model, operated by NOAA SWPC (http://wwwswpc.noaa.gov/products/d-region-absorption-predictions-d-rap), originally based on Sauer & Wilkinson (2008), using:

$$\mathrm{HAF} = (10 \log \mathrm{F} + 65) \cos^{0.75} (\mathrm{SZA})(\mathrm{MHz}), \qquad (2)$$

$$A_{\mathrm{SWF}} = 0.5 \left[\frac{\mathrm{HAF}}{30\,\mathrm{MHz}}\right]^{1.5} (\mathrm{dB}), \qquad (3)$$

where HAF is the highest affected frequency, F is the 0.1–0.8 nm solar X-ray flux, SZA is the solar zenith angle, and $A_{\mathrm{SWF}}$ is the absorption expected for a 30 MHz signal. At the MOD and SEV thresholds, $F_{\mathrm{MOD}}=10^{-4}$ Wm$^{-2}$ and $F_{\mathrm{SEV}}=10^{-3}$ Wm$^{-2}$. The maximum absorption expected, assuming the Sun is directly overhead, such that SZA = 0°, is 0.4 dB for MOD events and 0.6 dB for SEV events. These values are much smaller than expected based on the 2 dB and 5 dB thresholds characterizing PCA. The D-RAP model is known to underestimate observed absorption due to SWF (Schumer, 2009; Levine et al., 2019). Instead, consider absorption observed for MOD and SEV level events. Fiori et al. (2018) present an X2.1 solar X-ray flare observed on 11 March 2015 observed by a network of Canadian 30-MHz riometers. Observed absorption exceeded 1 dB at stations ranging from 45° to 63° geographic latitude on the dayside, with a maximum value of 2.4 dB at the lowest latitude station located in Ottawa, Canada, with a solar zenith
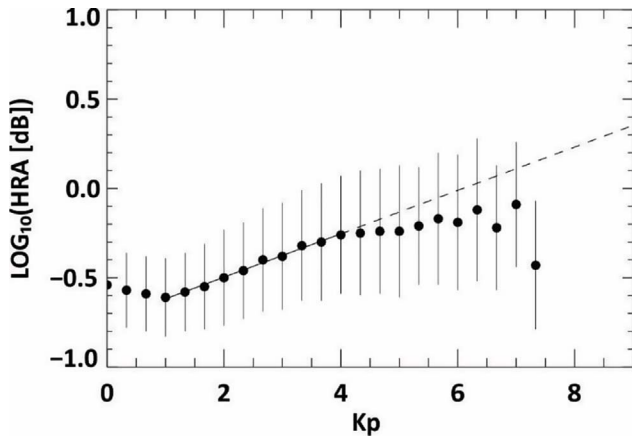
**Fig. 6.** Maximum hourly range of auroral absorption (HRA) versus Kp index binned in increments of 1/3 Kp. Filled circles and vertical lines indicate the mean and standard deviation of the HRA. Based on Fiori et al. (2020).

angle of 51.0°. Using the equations (2) and (3), this corresponds to maximum absorption of 4.0 dB at SZA = 0°. For the 03 July 2021 event, with an X1.6 flare, illustrated in Figure 3, maximum absorption of 1.6 dB observed at Ottawa (SZA = 62.1°) corresponds to maximum absorption of 3.6 dB at SZA = 0°. Absorption values of 3.6 dB and 4.0 dB at 30 MHz for a >X1 solar X-ray flare falls within the 2 dB and 5 dB thresholds set for PCA, and there is some consistency between SWF and PCA in terms of the expected impacts due to MOD and SEV absorption.

To evaluate auroral absorption at 30 MHz expected for Kp = 8 (MOD) and Kp = 9 (SEV), we consider the relationships presented in Fiori et al. (2020). It should be noted that Fiori et al. (2020) criticize the use of Kp for characterizing auroral absorption. Kp is a global geomagnetic activity index having a coarse 3-h resolution, based on data from sub-auroral stations. In contrast, auroral absorption is a highly dynamic phenomenon and tends to be observed at higher latitudes where observations reflect current systems not necessarily observed by the sub-auroral magnetic observatories contributing to the Kp index. They do, however, conclude that there is a general linear relationship between the logarithm of the hourly range of absorption (HRA) and Kp for Kp limited to values from 1 to 4. For Kp above this range, the relationship plateaus, partially due to a lack of statistics. Based on the tables presented in the Appendix of Fiori et al. (2020), Figure 6 shows the relationship between Kp and HRA. The solid line for Kp = [1, 4] represents a linear regression to the data, which is extended beyond Kp = 4 by a dashed line. As Kp increases, the regression line lies above the data but, with the exception of the last point, is within the error limits. From this line, the MOD (Kp = 8) and SEV (Kp = 9) event thresholds correspond to $HRA_{MOD} = 1.7$ dB and $HRA_{SEV} = 2.3$ dB, respectively. Given a mean event duration of 5.1 h for a MOD event, an increase of 1.7 dB absorption every hour until the maximum absorption is reached, and assuming absorption peaks exactly halfway through an event, then the maximum deviation for a MOD event is 4.3 dB. Similarly, given a mean event duration of 12.0 h for a SEV level event and an hourly increase of 2.3 dB absorption, the maximum deviation for a SEV event is 13.8 dB.

Auroral absorption thresholds for MOD and SEV PCA events can also be compared to observations during auroral absorption events for NRCan riometers operating after 2006. For the MOD 08 September, 2017 event observed at 12–15 UT, auroral zone riometers located at Cambridge Bay (CBB) (69° N, 105° W), Baker Lake (BLC) (64° N, 68° W), and Yellowknife (YKC) (62° N, 114° W) in Canada were located in the dawn sector. Clear absorption signatures were observed, peaking at 3.6 dB at CBB, 8.9 dB at BLC, and 7.0 dB at YKC. These values are not consistent with the 2 dB and 5 dB thresholds used for PCA and suggest the signal attenuation expected from a MOD or SEV level auroral absorption event exceeds, at least locally, the signal attenuation from an SWF or PCA event. Conversely, if the SWF and PCA thresholds are, in fact, representative of conditions at which HF COM is affected, then HF COM will be affected by auroral absorption before the MOD and SEV thresholds are crossed.

Impacted regions for the absorption events, when they occur, are unambiguous: dayside for SWF and high latitudes (~>60°) for AA (strongest impacts on the nightside) and PCA (strongest impacts on the dayside). In contrast, PSDs are both highly variable in space and time. For example, despite having measurements of ionospheric responses for several previous similar geomagnetic storms, it is still extremely difficult to predict the characteristic of the next PSD event associated with a similar type of geomagnetic storm. Based on a statistical analysis of several years of ionosonde data, Kumar & Parkinson (2017) attempted to provide the general characteristic of storm-time ionospheric depressions. The study concluded that PSD-type events are tied to the auroral region, and its equatorward expansion is regulated by two neutral wind systems; thermospheric winds, which are enhanced by storm-induced Joule heating, and background solar-induced winds, which are directed equatorward in the summer and poleward in the winter. The summer hemisphere may experience more widespread depression since the two wind systems are in-phase. Kumar & Parkinson (2017) also showed that the depressions tend to start immediately after the onset of geomagnetic storms in the nightside high-latitude region and can last for several tens of hours depending on storm intensity.

The PSD analysis shown here was based on only ionosonde data. Although the ionosonde data has been widely accepted as the best measure of ionospheric electron density, its sparse distribution and occasional problems in the ionogram scaling software may have contaminated some of the statistics presented here. However, the relative trend in the PSDs will not change. It would be ideal to repeat this analysis using long-term global maps of observed electron density, however, such a dataset is currently not available.

## 6 Summary and conclusions

Information about the occurrence rate and duration of space weather disturbances is necessary for space weather service centers to provide an operational service and for the industry to develop appropriate mitigation strategies. This paper examines the moderate (MOD) and severe (SEV) thresholds adopted by the International Civil Aviation Organization (ICAO) to identify events where space weather is likely to affect high-frequency

radio communication and evaluates the frequency and duration of events based on data sets spanning multiple solar cycles. Phenomena examined include absorption and post-storm maximum useable frequency depression (PSD).

Absorption was evaluated based on a 40-year data set spanning 1980–2020, representing >3 complete 11-year solar cycles. Absorption was sub-divided into three categories: short-wave fadeout (SWF), auroral absorption (AA), and polar cap absorption (PCA). All 3 absorption phenomena were shown to have occurrence trends that follow the solar cycle with peak occurrence frequency during solar maximum.

The threshold for shortwave fadeout is defined in terms of the strength of the electromagnetic radiation from solar flares, as defined by the solar X-ray flux measurements. Solar X-ray flux was analyzed by considering all $\geq$C solar-X-ray flares. MOD and SEV events represented 0.8% and 0.03% of the data set, respectively. This corresponds to 123 MOD and 5 SEV events per 11-year solar cycle. Events were concentrated around solar maximum (84%) and during solar cycle 22 (51%). MOD events had a mean duration of 68 min, and SEV events had durations that were > 30 min, with a mean duration of 132 min. Mean separation of 29 days was observed between successive X-class flares, with a median separation of 3 days. Multiple X-class flares tend to be grouped together, often from the same active region on the Sun. The maximum separation of 4.2 years between subsequent X-class flares was observed over the solar minimum.

Thresholds for auroral absorption are based on the global Kp index. Based on an analysis of 40-years of 3-h Kp data, MOD (Kp = 8) and SEV (Kp = 9) represented 0.9% and 0.1% of data for disturbed times where Kp $\geq$ 4. Seventy-eight auroral absorption events were identified over the period studied, representing 438 h of MOD or SEV activity. Of these events, the maximum Kp reached MOD levels in 72 cases and SEV levels in 6 cases. This corresponds to, on average, 20 MOD and 2 SEV events over the 11-year solar cycle. As with SWF, the occurrence frequency of MOD and SEV level activity follows the solar cycle: 68% of the event were observed during solar maximum, and 47% of events were observed during both solar cycles 22 and 23. The mean event duration was 5.1 h for MOD events and 12 h for SEV events. The mean separation between events was 177 days, with a maximum separation of ~5 years observed over the solar minimum.

MOD and SEV thresholds for polar cap absorption are based on the observed attenuation (absorption) observed for a 30 MHz signal. The thresholds are 2 dB and 5 dB for MOD and SEV events, respectively. Modeled absorption, calculated using the D-RAP model, was evaluated for solar proton events observed from 1986 to 2020. PCA events were identified as at least 3 consecutive 5-min intervals of $\geq$2 dB, allowing a gap of up to 3-h between consecutive intervals of $\geq$2 dB absorption. There were 115 events observed. Of these, 75 surpassed the MOD threshold, and 40 were SEV. This corresponds to 24 MOD and 13 SEV events over an 11-year solar cycle. 74% of events were observed during solar maximum, and 51% of events were observed during solar cycle 23. Event duration was the longest for the PCA event, with a mean duration of 7.85 h for MOD events and 1.6 days for SEV events. The maximum duration was 7.4 days. The separation between consecutive events ranged from 3.25 h to 4.6 years, with a median separation of 90 days.

The impact of the three types of absorption phenomenon on HF COM for MOD and SEV event thresholds was normalized by evaluating the absorption expected at 30 MHz due to SWF and AA-type absorption for comparison with PCA thresholds. Based on an analysis of one event, SWF-type absorption was shown to fall within the 2 dB and 5 dB range described for MOD and SEV PCA-type absorption. Auroral absorption was demonstrated not to be consistent with these results as absorption in excess of the SEV threshold was shown to be observed during a MOD-level event. This inconsistency suggests that the Kp thresholds used to define MOD and SEV auroral absorption may actually represent absorption levels considerably greater than MOD and SEV levels for the other types of absorption; equivalent effects might be observed for lower Kp than defined by current thresholds.

Statistics for HF post-storm depression were based on a 2-solar cycle (22-year) period of ionosonde observations. PSD events were counted if they occurred within 96 h after a Kp $\geq$ 6 events. For the 22-year study interval, 2186 h (91 days; 1.1% occurrence) of MOD events and 957 h (~40 days; 0.5% occurrence) of SEV events were identified. The median lifetime of MOD and SEV PSD events were found to be 5.5 and 8.5 h, respectively. The occurrence rate of PSD events closely followed the solar cycle, with a higher number of events occurring during solar maximum (62%) and close to zero events per month occurring during solar minimum. Events were most commonly observed during solar cycle 22 (66%) compared to solar cycle 23 (34%). The highest incidence of PSD events occurred in May 1991, when HF COM was impacted by space weather ~20% of the time.

Identification of the occurrence frequency and typical duration of absorption and post-storm depression events likely to impact high-frequency radio wave communication used by aviation is a valuable input to the development of both risk mitigation strategies and operational services for the industry.

# References

Baker DN, Stauning P, Hones EW Jr, Higbie PR, Belian RD. 1981. Near-equatorial, high-resolution measurements of electron precipitation at L ≈ 6.6. *J Geophys Res* **86**: A4. https://doi.org/10.1029/JA086iA04p02295.

Basler RP. 1963. Radio wave absorption in the auroral ionosphere. *J Geophys Res* **68**: 16. https://doi.org/10.1029/JZ068i016p04665.

Belrose J, Cetiner E. 1962. Measurement of electron densities in the ionospheric D-region at the time of a 2+ solar flare. *Nature* **195**: 688–690. https://doi.org/10.1038/195688a0.

Berngardt OI, Ruohoniemi JM, Nishitani N, Shepherd SG, Bristow WA, Miller ES. 2018. Attenuation of decameter wavelength sky noise during X-ray solar flares in 2013–2017 based on the observations of midlatitude radars. *J Atmos Sol-Terr Phys* **173**: 1–13. https://doi.org/10.1016/j.jastp.2018.03.022.

Bilitza D, Altadill D, Truhlik V, Shubin V, Galkin I, Reinisch B, Huang X. 2017. International reference ionosphere 2016: From ionospheric climate to real-time weather predictions. *Space Weather* **15**: 2. https://doi.org/10.1002/2016SW001593.

Boteler DH. 2018. Chapter 26 – dealing with space weather: The Canadian experience. In: *Extreme events in geospace*, Buzulukova N (Ed.), Elsevier, pp. 635–656. ISBN 9780128127001, https://doi.org/10.1016/B978-0-12-812700-1.00026-1. https://www.sciencedirect.com/science/article/pii/B9780128127001000261.

Brodrick D, Tingay S, Wieringa M. 2005. X-ray magnitude of the 4 November 2003 solar flare inferred from the ionospheric attenuation of the galactic radio background. *J Geophys Res* **110**: A09S36. https://doi.org/1029/2004JA010960.

Buonsanto MJ. 1999. Ionospheric storms – A review. *Space Sci Rev* **88**: 563–601. https://doi.org/10.1023/A:1005107532631.

Cameron D. 2012. *Delta reroutes flights as solar storm hits Earth*, Wall Street Journal, 25 January 2012. Available online at: http://www.wsj.com/articles/SB10001424052970203806504577181133714653496.

Cannon P, Angling M, Barclay L, Curry C, Dyer C, Edwards R, Greene G, Hapgood M, Horne R, Jackson D, Mitchell C, Owen J, Richards A, Rogers C, Ryden K, Saunders S, Sweeting M, Tanner R, Thomson A, Underwood C. 2013. *Extreme space weather: impacts on engineered systems and infrastructure*. Royal Academy of Engineering, London.

Chakraborty S, Ruohoniemi JM, Baker JBH, Nishitani N. 2018. Characterization of short-wave fadeout seen in daytime SuperDARN ground scatter observations. *Radio Sci* **53**: 4. https://doi.org/10.1002/2017RS006488.

Cherniak I, Zakharenkova I, Braun J, Wu Q, Pedatella N, Schreiner W, Weiss J-P, Hunt D. 2021. Accuracy assessment of the quiet-time ionospheric F2 peak parameters as derived from COSMIC-2 multi-GNSS radio occultation measurements. *J Space Weather Space Clim* **11**: 18. https://doi.org/10.1051/swsc/2020080.

Coyne VJ (Ed.). 1979. Special topics in HF propagation. In: *AGARD Conf. Proc. No. 263, Advisory Group for Aerospace Research and Development*, North Atlantic Treaty Organization, Printed by Technical Editing and Reproduction Ltd, Harford House, 7-9 Charlotte St, London.

Danilov AD. 2013. Ionospheric F-region response to geomagnetic disturbances. *Adv Space Res* **52**: 3. https://doi.org/10.1016/j.asr.2013.04.019.

Davies K. 1990. *Ionospheric radio*, IEE Electromagn. Ser., Peter Peregrinus, London, Vol. **31**.

Driatsky VM. 1966. Study of the space and time distribution of auroral absorption according to observations of the riometer network in the Arctic. *Geomagn Aeron* **6**: 828–834.

Fiori RAD, Koustov AV, Chakraborty S, Ruohoniemi JM, Danskin DW, Boteler DH, Shepherd SG. 2018. Examining the potential of the super dual auroral radar network for monitoring the space weather impact of solar X-Ray flares. *Space Weather* **16**: 1348–1362. https://doi.org/10.1029/2018SW001905.

Fiori RAD, Trichtchenko L, Balch C, Spanswick E, Groleau S. 2020. Characterizing auroral-zone absorption based on global Kp and regional geomagnetic hourly range indices. *Space Weather* **18**: 12. https://doi.org/10.1029/2020SW002572.

Foppiano AJ, Bradley PA. 1983. Prediction of auroral absorption of high-frequency waves at oblique incidence. *Telecommun J* **50**: 10.

Foppiano AJ, Bradley PA. 1984. Day-to-day variability of riometer absorption. *J Atmos Terr Phys* **46**: 8. https://doi.org/10.1016/0021-9169(84)90130-2.

Frank-Kamenetsky A, Troshichev O. 2012. A relationship between the auroral absorption and the magnetic activity in the polar cap. *J Atmos Sol-Terr Phys* **77**: 40–45. https://doi.org/10.1016/j.jastp.2011.11.007.

Frissell NA, Miller ES, Kaeppler SR, Ceglia F, Pascoe D, Sinanis N, Smith P, Williams R, Shovkoplyas A. 2014. Ionospheric sounding using real-time amateur radio reporting networks. *Space Weather* **12**: 651–656. https://doi.org/10.1002/2014SW001132.

Frissell NA, Vega JS, Markowitz EM, Gerrard AJ, Engelke WD, Erickson PJ, Miller ES, Luetzelschwab RC, Bortnik J. 2019. High-frequency communications response to solar activity in September 2017 as Observed by Amateur radio networks. *Space Weather* **17**: 118–132. https://doi.org/10.1029/2018SW002008.

Fuller-Rowell TJ, Codrescu MN, Rishbeth H, Moffett RJ, Quegan S. 1996. On the seasonal response of the thermosphere and ionosphere to geomagnetic storms. *J Geophys Res* **101**: 2343–2353. https://doi.org/10.1029/95JA01614.

Goodman JM. 1992. *HF communications – science and technology*, Van Norstrand Reinhold, New York.

Hargreaves JK. 1966. On the variation of auroral radio absorption with geomagnetic activity. *Planet Space Sci* **14**: 991–1006. https://doi.org/10.1016/0032-0633(66)90136-X.

Hargreaves JK. 1969. Auroral absorption of HF radio waves in the ionosphere: A review of results from the first decade of riometry. *Proc IEEE* **57(8)**: 1348–1373. https://doi.org/10.1109/PROC.1969.7275.

Hargreaves JK. 2005. A new method of studying the relation between ionization rates and radio-wave absorption in polar-cap absorption events. *Ann Geophys* **23**: 359–369. https://doi.org/10.5194/angeo-23-359-2005.

Hargreaves JK. 2010. Auroral radio absorption: The prediction question. *Adv Space Res* **45**: 1075–1092. https://doi.org/10.1016/j.asr.2009.10.026.

Hargreaves JK, Cowley FC. 1967. Studies of auroral radio absorption events at three magnetic latitudes – I. Occurrence and statistical properties of the events. *Planet Space Sci* **15**: 1571–1583. https://doi.org/10.1016/0032-0633(67)90090-6.

Hargreaves JK, Shirochkov AV, Farmer AD. 1993. The polar cap absorption event of 19–21 March 1990: Recombination coefficients, the twilight transition and the midday recovery. *J Atmos Terr Phys* **55**: 6.

Hartz TR, Montbriand LE, Vogan EL. 1963. A study of auroral absorption at 30 MC/S. *Can J Phys* **41**: 581–595. https://doi.org/10.1139/p63-061.

Holt C, Landmark B, Lied F. 1961. Analysis of riometer observations obtained during polar radio blackouts. *J Atmos Terr Phys* **23**: 229–243. https://doi.org/10.1016/0021-9169(61)90048-4.

Hosokawa K, Iyemori T, Yukimatu AS, Sato N. 2000. Characteristics of solar flare effect in the high-latitude ionosphere as observed by the SuperDARN radars. *Adv Pol Up Atmos Res* **14**: 66–75.

Hunsucker RD, Hargreaves JK. 2003. *The high-latitude ionosphere and its effects on radio propagation*. Cambridge atmospheric and space science series, Cambridge University Press, Cambridge.

ICAO. 2018. *Annex 3 to the Convention on International Civil Aviation, Meteorological Service for International Air Navigation*, ICAO International Standards and Recommended Practices, Twentieth Edition, July 2018, http://store.icao.int/products/annex-3-meteorological-service-for-international-air-navigation (last accessed 11 June 2020).

ICAO. 2019. *Manual on Space Weather Information in Support of International Air Navigation*, ICAO Doc 10100, First Edition, https://store.icao.int/products/manual-on-space-weather-informa-tion-in-support-of-international-air-navigation-doc-10100 (last accessed 11 June 2020).

Kauristie K, Andries J, Beck P, Berdermann J, Berghmans D, et al. 2021. Space weather services for civil aviation - challenges and solutions. *Remote Sens* **13**: 3685. https://doi.org/10.3390/rs13183685.

Kavanagh AJ, Marple SR, Honary F, McCrea IW, Senior A. 2004. On solar protons and polar cap absorption: constraints on an empirical model. *Ann Geophys* **22**: 3. https://doi.org/10.5194/angeo-22-1133-2004.

Knipp DJ, Bernstein V, Wahl K, Hayakawa H. 2021. Timelines as a tool for learning about space weather storms. *J Space Weather Space Clim* **11**: 29. https://doi.org/10.1051/swsc/2021011.

Kouznetsov A, Knudsen DJ, Donovan EF, Spanswick E. 2014. Dynamics of the correlation between polar cap radio absorption and solar energetic proton fluxes in the interplanetary medium. *J Geophys Res* **119**: 1627–1642. https://doi.org/10.1002/2013JA019024.

Kumar VV, Parkinson ML. 2017. A global scale picture of ionospheric peak electron density changes during geomagnetic storms. *Space Weather* **15**: 637–652. https://doi.org/10.1002/2016SW001573.

Levine EV, Sultan PJ, Teig LJ. 2019. A parameterized model of X-ray solar flare effects on the lower ionosphere and HF propagation. *Radio Sci* **54**: 168–180. https://doi.org/10.1029/2018RS006666.

Lu G, Richmond AD, Roble RG, Emery BA. 2001. Coexistence of ionospheric positive and negative storm phases under northern winter conditions: A case study. *J Geophys Res* **106**: 24493–24504. https://doi.org/10.1029/2001JA000003.

Matzka J, Bronkalla O, Tornow K, Elger K, Stolle C. 2021a. *Geomagnetic Kp index. V. 1.0*, GFZ Data Services. https://doi.org/10.5880/Kp.0001.

Matzka J, Stolle C, Yamazaki Y, Bronkalla O, Morschhauser A. 2021b. The geomagnetic Kp index and derived indices of geomagnetic activity. *Space Weather* **19**: 5. https://doi.org/10.1029/2020SW002641.

Mendillo M. 2006. Storms in the ionosphere: Patterns and processes for total electron content. *Rev Geophys* **44**: 4. https://doi.org/10.1029/2005RG000193.

Mitra A. 1974. *Ionospheric effects of solar flare*, Vol. **46**, Astrophysics and space science library, Reading, Massachusetts. https://doi.org/10.1007/978-94-010-2231-6.

National Research Council. 2008. *Severe space weather events – Understanding societal and economic impacts: A workshop report*. Natl. Acad. Press, Washington, D.C., 144 p.

Newell PT, Greenwald RA, Ruohoniemi JM. 2001. The role of the ionosphere in aurora and space weather. *Rev Geophys* **39**: 2. https://doi.org/10.1029/1999RG000077.

NOAA. 2004. *NOAA Intense Space Weather Storms October 19-November 07, 2003*, NOAA National Weather Service, U.S. Department of Commerce Report, Silver Spring, MD.

Prölss GW. 1995. Ionospheric F-region storms. In: *Handbook of atmospheric electrodynamics, Vol. 2*, Volland H. (Ed.), Chap. **8**, CRC Press. Boca Raton, Fla, pp. 195–235.

Prölss GW. 2008. Ionospheric storms at mid-latitude: A short review. In: *Midlatitude ionospheric dynamics and disturbances*, Kintner PM Jr., Coster AJ, Fuller-Rowell T, Mannucci AJ, Mendillo M, Heelis R (Eds.), Geophys. Monogr. Ser., Vol. **181**, AGU. Washington, D.C., pp. 9–24. https://doi.org/10.1029/181GM03. https://agupubs.onlinelibrary.wiley.com/doi/10.1029/181GM03.

Prölss G, Werner S. 2002. Vibrationally excited nitrogen and oxygen and the origin of negative ionospheric storms. *J Geophys Res* **107**: A2. https://doi.org/10.1029/2001JA900126.

Redmon RJ, Seaton DB, Steenburgh R, He J, Rodriguez JV. 2018. September 2017's geoeffective space weather and impacts to Caribbean radio communications during hurricane response. *Space Weather* **16**: 9. https://doi.org/10.1029/2018SW001897.

Sauer H, Wilkinson DC. 2008. Global mapping of ionospheric HF/VHF radio wave absorption due to solar energetic protons. *Space Weather* **6**: S12002. https://doi.org/10.1029/2008SW000399.

Schumer EA. 2009. *Improved modeling of midlatitude D-region ionospheric absorption of high frequency radio signals during solar X-ray flares*, PhD Dissertation, AFIT/DS/ENP/09-J01, U.S. Air Force, Wright-Patterson Air Force Base, Ohio.

Schwentek H. 1961. Short wave fadeouts, their modes and complete characterization. *J Atmos Sol-Terr Phys* **23**: 68–84. https://doi.org/10.1016/0021-9169(61)90033-2.

Sergeev VA, Shukhtina MA, Stepanov NA, Rogov DD, Nikolaev AV, Spanswick E, Donovan E, Raita T, Kero A. 2020. Toward the reconstruction of sub-storm-related dynamical pattern of the radiowave auroral absorption. *Space Weather* **18**: 3. https://doi.org/10.1029/2019SW002385.

Sigernes F, Dyrland M, Brekke P, Chernouss S, Lorentzen DA, Oksavik K, Deehr CS. 2011. Two methods to forecast auroral displays. *J Space Weather Space Clim* **1**: A03. https://doi.org/10.1051/swsc/2011003.

Starkov GV. 1994. Mathematical model of the auroral boundaries. *Geomagn Aeron* **34**: 3.

Stonehocker GH. 1970. Advanced telecommunication forecasting technique. In: *AGY, 5th., Ionospheric Forecasting, AGARD Conf. Proc*, Vol. **29**, pp. 27–31.

Swalwell B, Dalla S, Kahler S, White SM, Ling A, Viereck R, Veronig A. 2018. The reported durations of GOES soft X-ray flares in different solar cycles. *Space Weather* **16**: 6. https://doi.org/10.1029/2018SW001886.

Tesema F, Partamies N, Tyssøy HN, Kero A, Smith-Johnsen C. 2020. Observations of electron precipitation during pulsating aurora and its chemical impact. *J Geophys Res* **125**: 6. https://doi.org/10.1029/2019JA027713.

Tulasi Ram S, Liu CH, Su S-Y. 2010. Periodic solar wind forcing due to recurrent coronal holes during 1996–2009 and its impact on Earth's geomagnetic and ionospheric properties during the extreme solar minimum. *J Geophys Res* **115**: A12340. https://doi.org/10.1029/2010JA015800.

Watanabe K, Nishitani N. 2013. Study of ionospheric disturbances during solar flare events using the SuperDARN Hokkaido radar. *Adv Pol Sci* **24**: 1. https://doi.org/10.3724/SP.J.1085.2013.00012.

Zaalov NY, Moskaleva EV. 2016. A polar cap absorption model optimization based on the vertical ionograms analysis. *Adv Space Res* **58**: 9. https://doi.org/10.1016/j.asr.2016.07.024.

# Appendix

**Table A.1.** List of events where the maximum global polar cap absorption was >2 dB at 30 MHz. Event onset and end are indicated in YYYY–MM–DD HH:MM format. Data were evaluated at 5-min increments. Grey shading indicates events observed during solar maximum years, similar to Figure 2a.

| Event onset | Event end | Event onset | Event end |
|---|---|---|---|
| 1989-03-12 19:10 | 1989-03-13 11:25 | 2002-04-21 04:55 | 2002-04-21 13:00 |
| 1989-03-18 03:15 | 1989-03-18 04:10 | 2002-04-21 20:35 | 2002-04-22 12:30 |
| 1989-03-18 07:30 | 1989-03-19 11:45 | 2002-04-22 16:40 | 2002-04-22 17:55 |
| 1989-04-11 22:50 | 1989-04-12 06:10 | 2002-04-23 04:50 | 2002-04-23 05:30 |
| 1989-04-13 02:10 | 1989-04-13 08:10 | 2002-05-23 04:20 | 2002-05-23 05:05 |
| 1989-08-12 19:10 | 1989-08-15 01:35 | 2002-05-23 08:50 | 2002-05-23 11:55 |
| 1989-08-15 07:55 | 1989-08-18 09:50 | 2002-05-23 15:50 | 2002-05-23 17:15 |
| 1989-08-20 00:25 | 1989-08-20 10:50 | 2002-07-17 11:10 | 2002-07-17 20:00 |
| 1989-09-29 13:40 | 1989-10-01 15:20 | 2002-08-24 08:20 | 2002-08-24 09:00 |
| 1989-10-19 15:35 | 1989-10-27 00:20 | 2002-09-07 16:40 | 2002-09-07 18:35 |
| 1989-11-30 16:00 | 1989-11-30 23:25 | 2002-11-10 05:25 | 2002-11-10 06:35 |
| 1989-12-01 02:55 | 1989-12-02 00:50 | 2003-05-29 14:30 | 2003-05-29 19:15 |
| 1990-03-19 09:55 | 1990-03-20 23:00 | 2003-10-26 19:45 | 2003-10-27 06:25 |
| 1990-05-22 05:20 | 1990-05-22 08:05 | 2003-10-28 12:55 | 2003-10-31 03:15 |
| 1990-06-12 17:00 | 1990-06-12 20:30 | 2003-11-02 19:25 | 2003-11-04 11:55 |
| 1990-08-01 13:55 | 1990-08-02 05:25 | 2003-11-05 07:40 | 2003-11-05 08:40 |
| 1991-01-31 14:00 | 1991-01-31 22:20 | 2004-07-26 18:15 | 2004-07-27 03:05 |
| 1991-03-23 10:30 | 1991-03-26 08:30 | 2004-09-13 22:00 | 2004-09-14 15:45 |
| 1991-03-26 11:45 | 1991-03-26 12:25 | 2004-11-07 20:40 | 2004-11-08 11:55 |
| 1991-05-13 05:55 | 1991-05-13 15:45 | 2004-11-08 18:50 | 2004-11-08 21:00 |
| 1991-06-04 14:40 | 1991-06-04 16:05 | 2004-11-10 07:10 | 2004-11-10 11:00 |
| 1991-06-06 22:10 | 1991-06-07 14:25 | 2004-11-10 16:25 | 2004-11-10 21:30 |
| 1991-06-07 17:50 | 1991-06-09 02:55 | 2005-01-16 14:35 | 2005-01-17 00:15 |
| 1991-06-09 16:10 | 1991-06-09 16:25 | 2005-01-17 09:25 | 2005-01-18 23:00 |
| 1991-06-10 17:00 | 1991-06-10 17:40 | 2005-01-20 07:00 | 2005-01-20 22:20 |
| 1991-06-11 04:50 | 1991-06-13 10:15 | 2005-01-21 12:55 | 2005-01-21 18:30 |
| 1991-06-15 10:55 | 1991-06-16 17:50 | 2005-05-14 12:35 | 2005-05-15 06:15 |
| 1991-06-16 22:20 | 1991-06-17 04:20 | 2005-08-23 00:25 | 2005-08-24 10:45 |
| 1991-06-17 08:05 | 1991-06-17 11:20 | 2005-09-09 03:00 | 2005-09-12 09:20 |
| 1991-07-08 03:00 | 1991-07-09 06:20 | 2005-09-14 06:25 | 2005-09-14 20:10 |
| 1991-08-27 16:30 | 1991-08-28 04:45 | 2005-09-14 23:45 | 2005-09-15 03:50 |
| 1992-05-09 17:20 | 1992-05-10 10:25 | 2005-09-15 07:10 | 2005-09-15 14:45 |
| 1992-10-30 20:40 | 1992-11-01 23:15 | 2006-12-07 12:00 | 2006-12-08 20:20 |
| 1992-11-02 05:00 | 1992-11-03 05:25 | 2006-12-09 15:05 | 2006-12-09 15:40 |
| 1994-02-21 02:50 | 1994-02-21 12:35 | 2006-12-13 15:00 | 2006-12-13 17:00 |
| 1997-11-06 19:20 | 1997-11-07 16:05 | 2006-12-14 12:05 | 2006-12-14 17:40 |
| 1998-04-20 19:50 | 1998-04-22 22:40 | 2011-08-05 17:50 | 2011-08-05 22:45 |
| 1998-08-26 02:45 | 1998-08-26 19:45 | 2012-01-23 08:20 | 2012-01-25 07:20 |
| 1998-09-25 01:25 | 1998-09-25 01:55 | 2012-01-25 13:25 | 2012-01-25 17:50 |
| 1998-09-30 19:15 | 1998-10-01 17:00 | 2012-01-27 23:55 | 2012-01-28 05:45 |
| 1998-11-14 12:15 | 1998-11-14 15:25 | 2012-01-28 10:10 | 2012-01-28 22:50 |
| 2000-06-08 09:10 | 2000-06-08 15:10 | 2012-03-07 11:20 | 2012-03-10 05:40 |
| 2000-07-14 11:25 | 2000-07-16 07:35 | 2012-03-13 19:15 | 2012-03-14 06:25 |
| 2000-07-16 11:25 | 2000-07-16 13:10 | 2012-07-14 18:10 | 2012-07-14 22:10 |
| 2000-09-12 22:10 | 2000-09-13 06:00 | 2012-07-18 05:30 | 2012-07-18 06:05 |
| 2000-11-09 00:20 | 2000-11-10 19:40 | 2013-05-22 20:35 | 2013-05-23 19:35 |
| 2000-11-26 13:40 | 2000-11-26 23:25 | 2013-05-23 23:30 | 2013-05-24 00:20 |
| 2001-04-04 18:30 | 2001-04-04 19:05 | 2013-09-30 19:35 | 2013-10-02 02:35 |
| 2001-04-11 13:45 | 2001-04-12 03:35 | 2014-01-08 12:05 | 2014-01-09 07:05 |
| 2001-04-15 15:35 | 2001-04-15 16:10 | 2014-01-09 11:45 | 2014-01-09 20:30 |
| 2001-04-15 22:40 | 2001-04-16 02:55 | 2014-04-20 10:55 | 2014-04-20 11:10 |
| 2001-04-18 07:15 | 2001-04-18 11:25 | 2014-09-12 15:15 | 2014-09-12 17:30 |
| 2001-09-24 15:25 | 2001-09-28 17:10 | 2015-06-22 01:05 | 2015-06-23 02:10 |
| 2001-10-01 20:40 | 2001-10-02 22:20 | 2015-06-23 09:40 | 2015-06-23 10:15 |
| 2001-10-03 08:25 | 2001-10-03 09:15 | 2017-09-06 23:50 | 2017-09-07 12:50 |
| 2001-11-04 19:35 | 2001-11-05 00:35 | 2017-09-07 21:30 | 2017-09-08 05:50 |
| 2001-11-05 04:35 | 2001-11-07 01:15 | 2017-09-10 21:25 | 2017-09-12 12:50 |
| 2001-11-23 08:25 | 2001-11-24 20:15 | | |